Available online at www.sciencedirect.com
SCIENCE DIRECT®
Acta Materialia 52 (2004) 271–284
Acta MATERIALIA
www.actamat-journals.com

A coupled atomistics and discrete dislocation plasticity simulation of nanoindentation into single crystal thin films

Ronald E. Miller [a,*], L.E. Shilkrot [b], William A. Curtin [b]

[a] Department of Mechanical and Aerospace Engineering, Carleton University, 1125 Colonel By Dr., Ottawa, Ont., Canada, K1S 5B6
[b] Division of Engineering, Brown University, Providence, RI 02912, USA

Received 23 May 2003; received in revised form 8 September 2003; accepted 12 September 2003

Abstract

The phenomenon of 2D nanoindentation of circular ''Brinell'' indenter into a single crystal metal thin film bonded to a rigid substrate is investigated. The simulation method is the coupled atomistics and discrete dislocation (CADD) model recently developed by the authors. The CADD model couples a continuum region containing any number of discrete dislocations to an atomistic region, and permits accurate, automatic detection and passing of dislocations between the atomistic and continuum regions. The CADD model allows for a detailed study of nanoindentation to large penetration depths (up to 60 Å here) using only a small region of atoms just underneath the indenter where dislocation nucleation, cross-slip, and annihilation occur. Indentation of a model hexagonal aluminum crystal shows: (i) the onset of homogeneous dislocation nucleation at points away from the points of maximum resolved shear stress; (ii) size-dependence of the material hardness, (iii) the role of dislocation dissociation on deformation; (iv) reverse plasticity, including nucleation of dislocations on unloading and annihilation; (v) permanent deformation, including surface uplift, after full unloading; (vi) the effects of film thickness on the load–displacement response; and (vii) the differences between displacement and force controlled loading. This application demonstrates the power of the CADD method in capturing both long-range dislocation plasticity and short-range atomistic phenomena. The use of CADD permits for a clear study of the physical and mechanical influence of both complex plastic flow and non-continuum atomistic-level processes on the macroscopic response of material under indentation loading.

Keywords: Nanoindentation; Multiscale modelling; Atomistic simulation; Dislocations

1. Introduction

With the advent of nanostructured metals and MEMS devices, in which contacting surfaces can have nanoscale roughness and deformation, nanoindentation and related tools such as atomic force microscopy are evolving into important probes of material behavior at small scales. Micro- and nanoindentation on metals are showing evidence that size-dependent hardening occurs at small scales, in contradiction to the predictions of continuum plasticity. Furthermore, indentation on nanometer length scales is bringing experimental studies into the size range that may be accessible by atomistic simulations, suggesting the possibility of direct comparison between simulations and experiments. Of specific interest here are nanoindentation experiments on single- or polycrystals of ductile metals [4,9,10,14,26,31], where the primary deformation mode are the nucleation and long-range flow of dislocations. Several researchers have presented fully atomistic simulations of these experiments [3,13,16,17,21,28,32,33] using empirical potentials to describe atomic interactions. Simulation sizes range from 25,000 atoms on a single processor to several million atoms in parallel-computing environments. Most recently, a direct comparison between nanoindentation experiment and simulation was presented by de la Fuente et al. [7], whereby detailed scanning tunneling microscopy of dislocation-induced surface defects were combined with simulation to elucidate the mechanisms of plastic flow. In spite of the tantalizing

* Corresponding author. Tel.: +1-613-520-2600/5703; fax: +1-613-520-5715.
E-mail address: rmiller@mae.carleton.ca (R.E. Miller).

1359-6454/$30.00 © 2003 Acta Materialia Inc. Published by Elsevier Ltd. All rights reserved.
doi:10.1016/j.actamat.2003.09.011

possibility, atomistic simulation sizes are still too small to make direct comparisons with many relevant and important experiments. For instance, experimental evidence suggests a peak in the hardness of nanocrystalline metals for grain sizes in the range of 10–50 nm. Full atomistic studies on suitably represented polycrystals at this size scale remain a computational challenge. Hence, new multiscale approaches to bridging atomistic and continuum phenomena are necessary, and have been the subject of considerable study in recent years.

There are many examples in the literature of numerical modeling techniques whereby an atomistic region is directly coupled to a continuum region modeled by finite elements [1,15,20,22,30]. A recent review [5] has discussed in great detail the goal of such modeling techniques and elucidated many of their challenges and advantages. The coupled atomistics and discrete dislocation (CADD) method described in [19,24,25] is one such method, but it is unique in that the continuum region can contain discrete dislocations, so that deformation in the form of dislocation plasticity can extend well beyond the boundaries of the fully atomistic domain with no appreciable loss of accuracy in the problem under study. The CADD method thus allows for the modeling of phenomena where atomic scale defect nucleation and interaction effects are important, but where, at the same time, these defects will tend to move over long distances away from the regions that require full atomistics. Such problems include crack tip dislocation emission, dislocation nucleation at grain boundaries, and nanoindentation. Here, nanoindentation of a cylinder into a single crystal substrate is examined using the CADD method. Although the CADD formulation is currently limited to two-dimensional (2D) analysis, application of the model provides many useful insight into nanometer scale deformation mechanisms.

Nanoindentation into ductile, single crystal films is a problem well-suited to the CADD approach. There is a relatively small, well-defined region beneath the indenter tip where dislocation nucleation is likely to occur and thus where a fully atomistic treatment is necessary. On the other hand, a relatively large model is required to facilitate realistic boundary conditions, making a fully atomistic treatment computationally inefficient. A large simulation volume is also needed because nucleated dislocations can glide long distances from their point of nucleation due to the long-ranged stress field of the indenter. Moreover, such dislocations need not be treated atomistically once they are more than a few indenter radii from the region of indentation.

In this paper, nanoindentation into initially defect-free single crystals is analysed in detail using the CADD approach. The simulations allow us to observe the initial nucleation of defects below the surface of the indented crystal, and to correlate many features in the load–displacement with the nucleation, motion, cross-slip and pile-up of dislocations. In addition to the physical insights into the nanoindentation problem, the work demonstrates two important benefits of the CADD approach. First, the use of CADD successfully reduces the computational overhead from what would be required to perform the same simulations using a fully atomistic model. While the total number of atoms in our simulated crystals are typically on the order of about 200,000, the number of degrees of freedom (atoms, nodes and dislocations) in the CADD models never exceeded 7000. Second, the CADD framework facilitates interpretation of the results, due to the identification and tracking of each dislocation in the system. In contrast, typical atomistic simulations of indentation can only yield qualitative information about the nature of the dislocations, how they nucleate and how they move through the material. By taking advantage of CADD's improved ability to track dislocations, our study reveals the detailed evolution of the defect structure during indentation load–unload cycles.

The remainder of this paper is organized as follows. In Section 2, a brief overview of the CADD method is presented. In Section 3, the nanoindentation problem is described and the simulation results are presented and discussed. Section 4 contains closing remarks about the method and its applications.

2. The coupled atomistics and discrete dislocation model

The details of the CADD approach have been published previously, both in a short letter [24] and in full detail [25]. Thus, in this paper we provide only a brief description of the main ideas. The CADD method contains three main elements: a scheme to mechanically couple an atomistic region with a continuum region containing discrete dislocations, an algorithm to detect dislocations near the atomistic/continuum interface, and an algorithm to pass dislocations from the atomistic region to the continuum region, or vice versa.

We begin with the atomistic/continuum coupling. Fig. 1 illustrates the essential details of the CADD solution of a general boundary value problems (bvp). The body is divided into one or more atomistic regions Ω_A and one or more linear elastic, continuum regions Ω_C, with interfaces $\partial\Omega_I$ between atomistic and continuum regions. Tractions $\boldsymbol{T} = \boldsymbol{T}_0$ are prescribed on $\partial\Omega_T$ and displacements $\boldsymbol{u} = \boldsymbol{u}_0$ on $\partial\Omega_u$. Region Ω_C contains N continuum discrete dislocations, while the atomistic regions may contain any atomic scale defects (dislocations, grain boundaries, vacancies, voids, amorphous regions). The solution to this bvp consists of atom positions $\boldsymbol{r}_A$, dislocation positions $\boldsymbol{d}^i$ and continuum displacements $\boldsymbol{u}$, stresses $\boldsymbol{\sigma}$, and strains $\boldsymbol{\epsilon}$. It is obtained by considering separate problems in the continuum (in Fig. 1, Problems I and II) and atomistic (in Fig. 1,

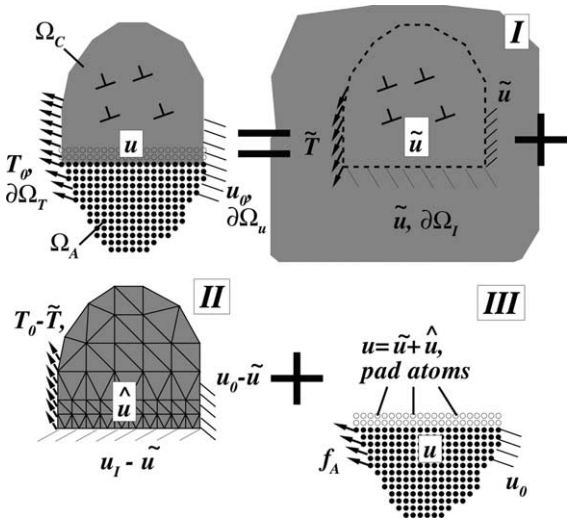

Fig. 1. Schematic illustration of the solution procedure for coupled atomistics and discrete dislocation plasticity. The continuum is coupled to the atomistic region by the displacements of the atoms on the interface, $\boldsymbol{u}_{\mathrm{I}}$, while the atoms are coupled to the continuum by the pad atoms whose displacements are dictated by the continuum fields.

Problem III) domains, generated by cutting the system along the interface $\partial\Omega_{\mathrm{I}}$ while enforcing continuity of displacements across $\partial\Omega_{\mathrm{I}}$. Because the method is designed to find equilibrium solutions to boundary value problems, the current implementation of CADD is a static, zero temperature model. All loading is quasi-static, achieved by incrementally increasing boundary loads or displacements on previous equilibrium solutions. A dynamic, finite temperature CADD model is the subject of current research.

The material properties of the model are determined from the underlying atomistic model employed. Here we use the "embedded atom method" (EAM) [6] interatomic potentials, although any model providing atomic forces can be used. The atomistic region is thus a fully nonlinear, non-local atomistic model that reduces exactly to lattice statics when no continuum region is appended. The continuum region requires the anisotropic elastic moduli, computed a priori from the atomistic model for an appropriately oriented crystal of the material. The continuum model also requires a list of all dislocation Burger's vectors permitted to exist in the continuum, which is again determined from knowledge of the atomic structure.

The fields in the continuum region can be treated using the standard discrete dislocation (DD) method [27]. Specifically, the continuum problem is divided into two complementary problems (Fig. 1). Problem I consists of dislocations in an infinite elastic continuum and is solved by superposition of the analytical elastic fields due to the individual dislocations at positions $\boldsymbol{d}^i$, yielding a total field denoted as the $\tilde{}$ field. Problem I generates tractions $\tilde{\boldsymbol{T}}$ along $\partial\Omega_{\mathrm{T}}$ and displacements $\tilde{\boldsymbol{u}}$ and $\tilde{\boldsymbol{u}}_{\mathrm{I}}$ along $\partial\Omega_{\mathrm{u}}$ and $\partial\Omega_{\mathrm{I}}$ that differ from the values of $\boldsymbol{T}_0$ and $\boldsymbol{u}_0$ prescribed by the boundary conditions and the $\boldsymbol{u}_{\mathrm{I}}$ imposed by the atomistic region. Problem II consists of a linear elastic continuum with no dislocations but subject to "corrective" tractions $\hat{\boldsymbol{T}} = \boldsymbol{T}_0 - \tilde{\boldsymbol{T}}$ on $\partial\Omega_{\mathrm{T}}$ and displacements $\hat{\boldsymbol{u}} = \boldsymbol{u}_0 - \tilde{\boldsymbol{u}}$ on $\partial\Omega_{\mathrm{u}}$ and $\hat{\boldsymbol{u}} = \boldsymbol{u}_{\mathrm{I}} - \tilde{\boldsymbol{u}}_{\mathrm{I}}$ on $\partial\Omega_{\mathrm{I}}$. All discontinuities and singularities of the dislocations are contained in the $\tilde{}$ fields of Problem I, so the fields of Problem II, denoted as $\hat{}$ fields, are smooth and obtainable numerically by the finite element method. The total fields in the continuum are the superposition of the fields from Problems I and II: $\boldsymbol{u} = \tilde{\boldsymbol{u}} + \hat{\boldsymbol{u}}$, $\boldsymbol{\sigma} = \tilde{\boldsymbol{\sigma}} + \hat{\boldsymbol{\sigma}}$ and $\boldsymbol{\epsilon} = \tilde{\boldsymbol{\epsilon}} + \hat{\boldsymbol{\epsilon}}$. For a given displacement along the atomistic/continuum interface $\partial\Omega_{\mathrm{I}}$, the stress in the continuum is used to obtain the Peach–Koehler force on each discrete dislocation. The displacement of any atom in the continuum region can be also be obtained using the reference crystal structure, the field $\tilde{\boldsymbol{u}}$, and the interpolated field $\hat{\boldsymbol{u}}$.

Forces on the atoms in Problem III are computed based on a physical interpretation of atomic forces in such a way that spurious forces at the atomistic/continuum interface are eliminated. First, the positions of the unfilled *pad atoms* in Fig. 1 are found from interpolation of the continuum displacement fields. This pad is at least twice the cutoff radius of the interatomic potentials to ensure that atoms on $\partial\Omega_{\mathrm{I}}$ do not "see" the free surface created by the cut. Forces on the atoms in Ω_{A} and on $\partial\Omega_{\mathrm{I}}$ are then the forces as obtained from a purely atomistic description of the material including the pad atoms.

With the forces on the atoms and dislocations obtained as described above, the system is then driven toward equilibrium using a force-based formulation and a "pseudo-conjugate gradient" (PCG) minimization scheme. A force-based method is required because there is no correct overall energy functional for the entire system. In the PCG, conjugate search directions are used at each iteration as in CG, but rather than seeking the minimum *energy* configuration along each line search, the system is moved to the configuration for which the projection of the *force vector* along the search direction is zero. At each step of the PCG minimization, all atoms in Ω_{A} and along $\partial\Omega_{\mathrm{I}}$ will move. The change in atomic positions along $\partial\Omega_{\mathrm{I}}$ alters the boundary conditions for the continuum region and hence alters the continuum fields; i.e., there is a mechanical coupling between the atomistic region and the continuum discrete dislocations. At the same time, the response of the continuum will include motion of the pad atom positions, which then generates forces on the atoms in Ω_{A} and on $\partial\Omega_{\mathrm{I}}$ and influences the subsequent atomic motions. There is no limit on the number of minimization steps, taken, but rather the minimization proceeds until the displacements of all atoms and nodes during a step are less than 10^{-6} Å.

Use of the pad atoms as an intermediary between the local continuum and the non-local, discrete atomistics

avoids problems that arise in previous atomistic/continuum coupling methods like the quasicontinuum. Such previous methods use an total-energy formulation, which leads to spurious relaxations at the atomistic/continuum interface due to so-called "ghost forces" [23]. The coupling method adopted here is essentially that of Kohlhoff et al. [15], except that we did not find it necessary to use nonlinear or non-local finite elements as employed by those researchers. Of course, the method of [15] did not allow for dislocations in the continuum region.

Dislocations in Ω_A that move toward Ω_C must be detected and "passed" to the continuum region. To accomplish this, we define a "detection band" of triangular elements (shown in Fig. 2) between atoms a few angstroms from the atomistic/continuum interface, just inside Ω_A. If a dislocation passes through one of these elements, it generates a signature Lagrangian finite strain in the element, which can be used to identify the Burgers vector and slip plane of the nucleated defect. The detection algorithm monitors the strains in the detection band elements and compares them to the possible dislocation slip strains for the crystal after each PCG energy minimization step. When the strain in an element corresponds to a particular dislocation, the dislocation core is assumed to reside at the centroid of that element. Because multiple dislocations can pass through one element, it is necessary to keep track of all previous slip activity and consider only the displacements due to new defects.

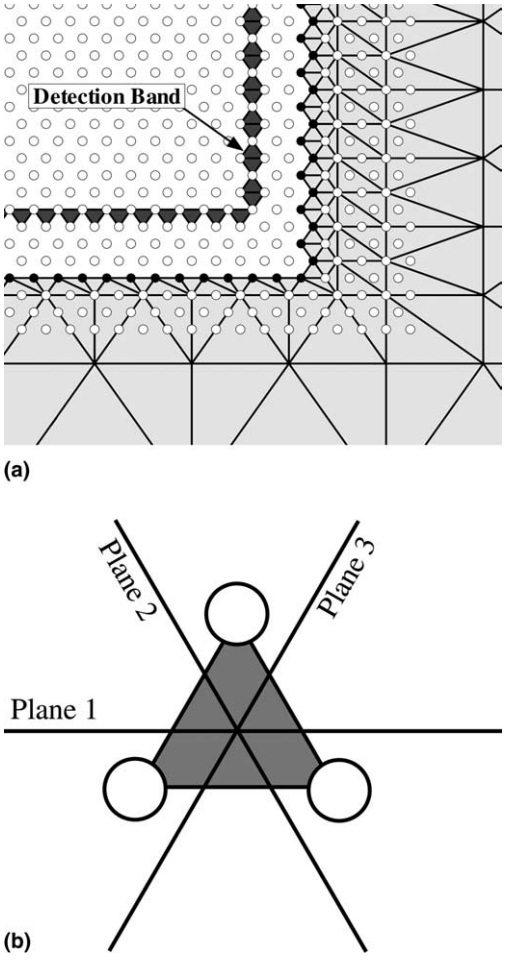

Fig. 2. (a) Close-up of the atomistic/continuum interface. Continuum elements are light grey. Dark grey elements are used in dislocation detection but do not contribute to the energy. The actual interface between the two regions is made up of the atom/nodes shown by filled circles, while unfilled circles that lie inside the continuum region are used as a "pad" of atoms to couple the atoms to the continuum region. (b) A close-up of one detection element, indicating the three slip planes on which it lies.

The detection algorithm establishes the location of the core, the slip plane, and the Burgers vector of the continuum entity. To "pass" the dislocation to Ω_C, the core is artificially shifted along its slip plane by adding the displacement fields associated with a dislocation dipole. These displacements cancel the original core in the atomistic region and add a new (continuum) core in the continuum region. Once this core is in the continuum region, it is added to the array of discrete dislocations with care being taken to define the branch-cut in the continuum displacement field such that it matches the slip plane along which the dislocation moves. Subsequent relaxation of the atoms naturally anneals out the remnants of the atomic core and moves the dislocation to its continuum equilibrium position. In a similar way, it is straightforward to pass dislocations from the continuum to the atomistic region.

3. "Brinell" nanoindentation

The indented material studied here is hexagonal Al with the c-axis normal to the in-plane deformation. The material is modeled using the EAM potentials of Ercolessi and Adams [8], with previously determined equilibrium lattice constant and in-plane elastic moduli of $a_0 = 2.83$ Å, $C_{11} = C_{22} = 0.9581$ eV/Å^3, $C_{12} = 0.5747$ eV/Å^3 and $C_{66} = 0.1917$ eV/Å^3. This hexagonal Al is unstable in out-of-plane shear, but such deformation is not permitted in the 2D calculations performed here. The hexagonal crystal provides a simplified model, but one with sufficient slip systems that some qualitative comparison to real crystals can be made. Specifically, the hexagonal crystal will contain only edge dislocations on three slip systems at 0°, 60° and −60°. The dislocation cores do not split into partials and can readily dissociate from one system onto the other two, a 2D analog of 3D cross-slip. As demonstrated in [24,25], CADD is also capable of modeling fcc crystals with mixed partial dislocations, but the added complexity does not provide additional insight into the indentation problem.

The indentation sample is a thin film of the hexagonal Al with its bottom surface bonded to a rigid substrate

and a free upper surface into which the indenter is pressed. Two models are considered as shown in Fig. 3: a "thick" film with $t = 941$ Å and a "thin" film with $t = 78.5$ Å. We simulate indentation by a rigid, frictionless, cylindrical indenter by defining a repulsive potential of the form

$$\Phi = \begin{cases} C(r-R)^2 & \text{for } r < R, \\ 0 & \text{for } r \geqslant R, \end{cases} \quad (1)$$

where $C = 100\,\text{eV/Å}^2$ is chosen empirically and $R = 100$ Å is chosen in this study as the indenter radius. The Al atoms interact with this potential, which effectively repels the atoms and forces them to remain outside the 100 Å radius of the indenter. This frictionless indenter, with no attractive interactions with the atoms, can be approximately achieved in experiments where the indenter tip is coated with a passivating layer (see, for example [14]). Loading is quasi-static, and is achieved in one of two ways. The first simulates a *displacement-controlled* nanoindentation experiment by incrementally moving the indenter position down, superimposing a uniform incremental compressive strain on the equilibrium solution from the previous load step, and then relaxing atoms, nodes, and continuum dislocations while holding the indenter position fixed. The second loading mimics a *force-controlled* nanoindentation experiment by incrementing the force applied to the indenter between relaxation steps.

3.1. Displacement-controlled indentation of the "thick" film

The load–displacement (P–δ) curve from the simulation of displacement-controlled indentation of the thick film is shown in Fig. 4 by the hollow squares. Critical points on the curve are labelled by roman numerals.

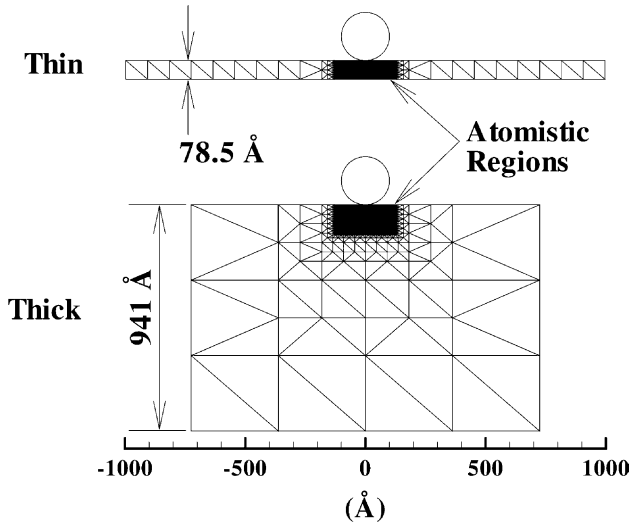

Fig. 3. Model geometries for the Brinell nanoindentation simulations. The radius of both indenters is 100 Å.

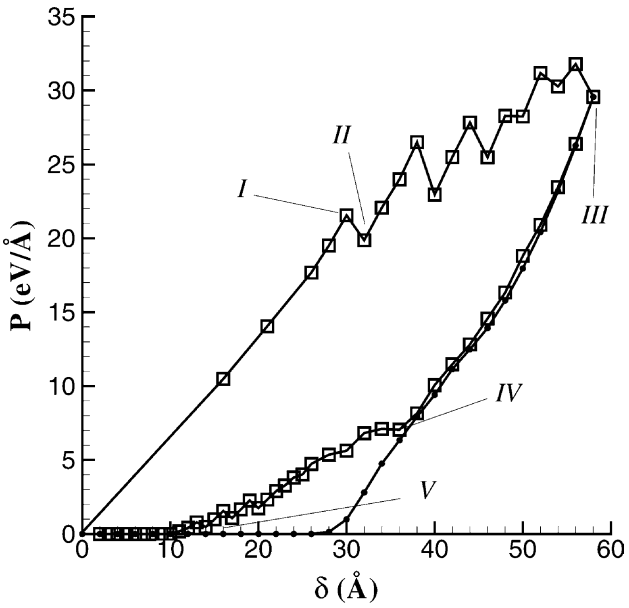

Fig. 4. Load–displacement curve for displacement-controlled indentation of the thick film shown as hollow squares. Points *I–V* are critical features described in the text. Filled circles show the effect of fixing the dislocations during unloading.

From the start of the loading to point I, the response is completely elastic. Using the contact area at I, the pressure distribution under the indenter is found to be in excellent agreement with the prediction of Hertzian contact theory, indicating that the film is sufficiently "thick" such that the rigid substrate is not affecting the elastic response.

The step from I to II corresponds to the first nucleation of dislocations. The nucleation process is elucidated in Fig. 5, which shows the equilibrated region under the indenter at points I (a) and II (b). Animated sequences of the nucleation process show that the two dipole pairs nucleate simultaneously at the encircled position, and immediately move along the slip planes located at $\pm 30°$ from the vertical. Two of these dislocations travel down and out the bottom of the atomistic region, where they are converted to discrete dislocations that eventually come to rest near the lower boundary of the model. The other two move up and hit the surface of the indenter, where they are reflected back into the crystal along a new slip plane. Note that in Fig. 5 and in subsequent images of the atomistic region, we will often show a finite element mesh joining the atoms, rather than the atoms themselves. This is helpful for visualization, as the mesh is defined in the reference, perfect lattice configuration. When deformation such as dislocation motion takes place, the heavily deformed elements clearly show the effect on the structure. Elements within the atomistic region are not used by the CADD simulation in computing forces or energy, they are only used for the visualization just described. Figs. 5(c) and (d) show an *intermediate*, *non-equilibrated* configuration

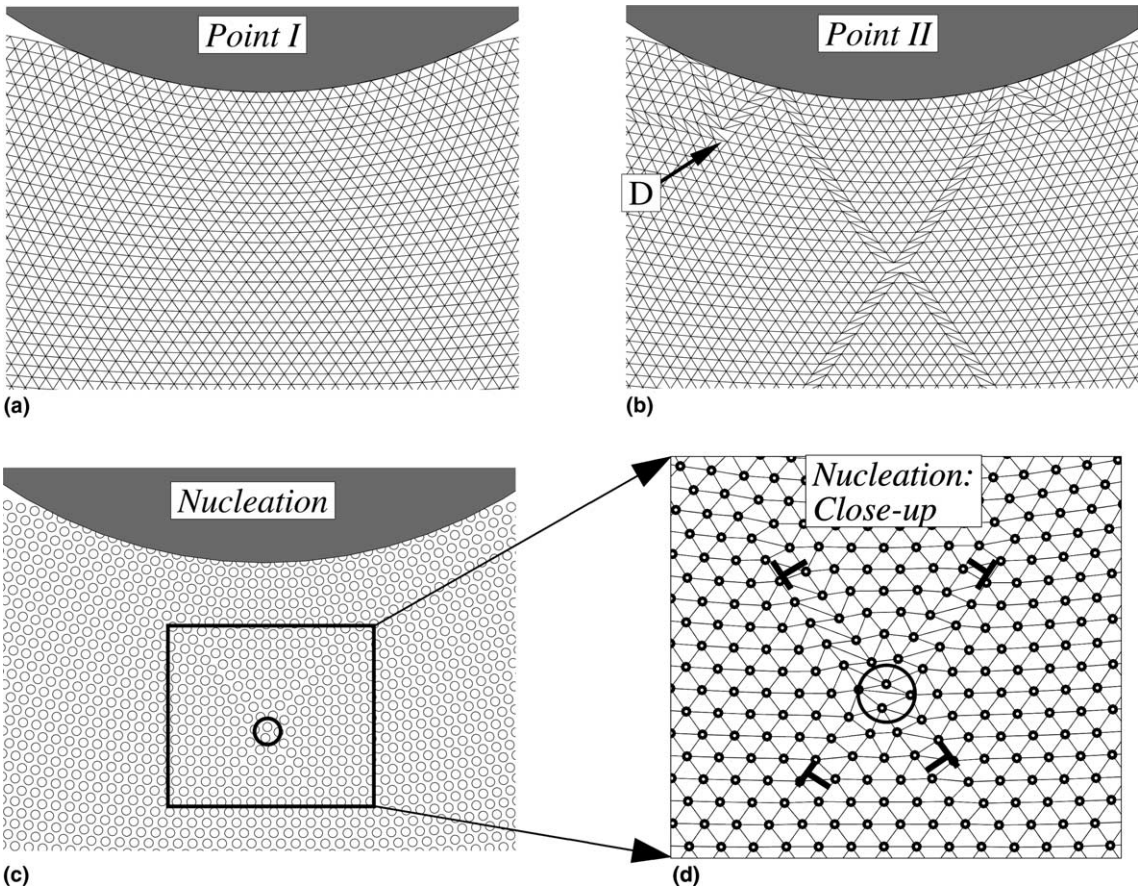

Fig. 5. Initial nucleation of a dislocation between points *I* and *II* on the *P*–δ curve. (a) Equilibrium configuration prior to nucleation. (b) Equilibrium configuration after nucleation. (c)–(d) Non-equilibrium intermediate configuration showing the nucleation process, which is initiated in the encircled region.

during the PCG minimization of the load increment from I to II. In (c), a low magnification view showing the atoms reveals the location of the first dislocation nucleation relative to the indenter, while the close-up in (d) shows the nucleation site in more detail with the emerging slip planes clearly observable via the superimposed mesh.

The nucleation site is located at a depth of approximately $0.86a$, where a is the half-width of the contact area between the film and the indenter. This is consistent with the depth of the maximum resolved shear stresses predicted by Hertzian theory ($0.78a$), but in fact the Hertzian maximum stresses occur on planes different from those on which the defects first form. Defining the maximum resolved shear stress on any of the three slip systems as

$$\tau_{\mathrm{r}}^{\max} = \max\left(\tau_{\mathrm{r}}^{1}, \tau_{\mathrm{r}}^{2}, \tau_{\mathrm{r}}^{3}\right), \tag{2}$$

where τ_{r}^{i} is the resolved shear stress on the ith slip system, Fig. 6 shows contours $\tau_{\mathrm{r}}^{\max}$, just prior to defect nucleation, as computed from the atomic level stresses.[1]

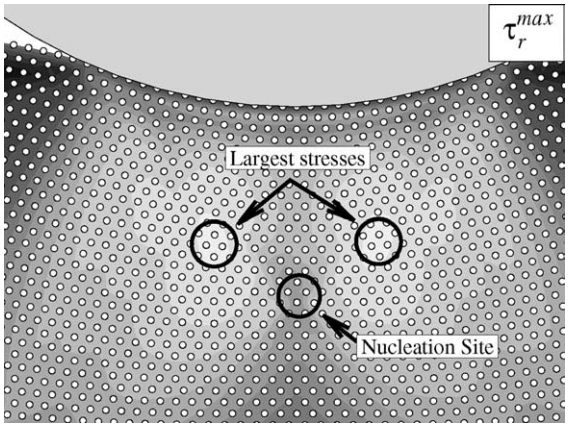

Fig. 6. Contours of the maximum critical resolved shear stress prior to dislocation nucleation. The largest values of $\tau_{\mathrm{r}}^{\max}$ are not located at the site of nucleation.

Clearly, the maximum stresses (the lightest contours) occur a significant distance from the actual nucleation site, indicating that the maximum resolved shear stress is not the correct parameter to predict nucleation. The fact that the maximum resolved shear stress on the possible slip planes is likely not to lie on the indenter axis was

[1] The stresses are the so-called "virial stresses", see for example [2].

recently pointed out by Kelchner et al. [13]. A number of researchers have recently proposed alternatives to the maximum stress criterion for dislocation nucleation [18,29] based on similar observations.

After nucleation, the dislocation moving up and to the left in Fig. 5(b) undergoes a dissociation at the point labelled *D*. This is a unique feature of the 2D hexagonal crystal structure used in the simulation, wherein a dislocation gliding on one of the three slip systems can dissociate into two dislocations, one on each of the other two systems. At *D* in Fig. 5(b), the dislocation travelling down and to the left (after having reflected off of the indented surface) dissociates into one dislocation that moves horizontally left and another that moves up and left. Such dissociation events occur frequently in the simulations described herein and can be viewed as a 2D analog to cross-slip in 3D, which is governed by competing stresses that drive dislocation glide in various directions.

Between points II and III, dislocation dipole pairs continue to nucleate and move out of the atomistic region. All the nucleation events occur at essentially the same location beneath the indenter. During this part of the loading process, the hardness H (load divided by the contact area) can be calculated from the equilibrated simulation results. In Fig. 7, we present the hardness obtained between stages I and III. The discrete nucleation events lead to dramatic variations in H, but in general the hardness decreases with increasing depth of indentation. A least-squares fit of the data to the form $H = H_0 + A\delta^{-1/2}$ is shown in Fig. 7, and provides reasonably good agreement. This functional form is consistent with a number of theoretical models that attempt to explain the indentation size effect (see, for example [12] and references therein). The model of [12], although it was developed to capture the indentation size effect at slightly larger length scales than presented here, may be applicable to the present results. In that model, the size effect is attributed to the changing ratio of surface and volume effects, and includes a detailed accounting of the various surface work and volume work terms. Most of the surface work contributions in that model are not present in our simulation (for example, the fracture of an oxide film). However, we note that our simulation includes a surface work term that is essentially the same as the work to form surface steps identified in [12]. Specifically, new surface is created during the process shown in Fig. 5(b), whereby the nucleated dislocations hit the indenter surface and are reflected back. This leaves a residual dislocation at the surface whose effect is to increase the surface area of the crystal. Further simulations of this type, the subject of future work, may be useful in testing this particular model of the indentation size effect.

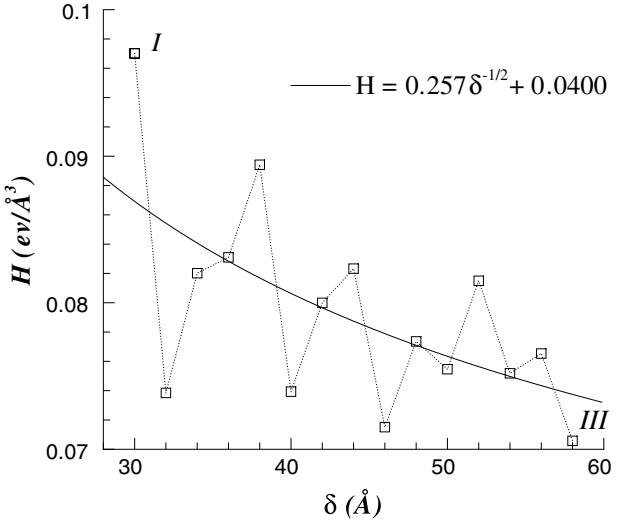

Fig. 7. Variation of hardness (load divided by contact area) with increasing indentation depth for the thick film.

At the peak load level applied here, point III of Fig. 4, the state of deformation is as shown in Fig. 8(a), at the atomistic scale, and (b) at the continuum scale where the discrete dislocations are shown as hollow circles. Clearly, a significant number of dislocations have moved out of the bottom of the atomistic region and have piled-up against the rigid lower boundary. Due to the large deformation state in the atomistics, however, these dislocations are not all on the same slip plane, which will have consequences for the unloading behavior. In addition, several dislocation have moved out of the left and right sides of the atomistic region due to the dissociation mechanism described above. The scale of the plasticity thus extends over nearly the entire sample volume. The application of CADD avoids the need for atomistic simulations containing 100,000 atoms or more, and in fact the CADD method could be applied here on much larger specimens with no appreciable increase in computational time or loss of accuracy.

Upon unloading from the peak load at point III, the continuum dislocations glide back toward the indenter, as evident by comparing the deformation states at points III and IV shown in Figs. 8(b) and (d), respectively. The total number of dislocations (continuum dislocations plus those inside the atomistic region) is not changing, however. Instead, the dislocations are simply gliding back into the atomistic region. The initial stage of unloading (between III and IV) departs slightly from linear elastic unloading, due to the motion of the dislocations back toward the interface, but in fact the effect of this plastic flow is rather small. The CADD method allows us to artificially hold the dislocations in the continuum region at fixed positions while unloading, so as to quantify the effect of the dislocation motion on the P–δ unloading response. The unloading curve so obtained is shown in Fig. 4 by the filled circles, and shows that the reverse motion of the dislocations has little effect on the unloading curve between points III and IV. The slope of

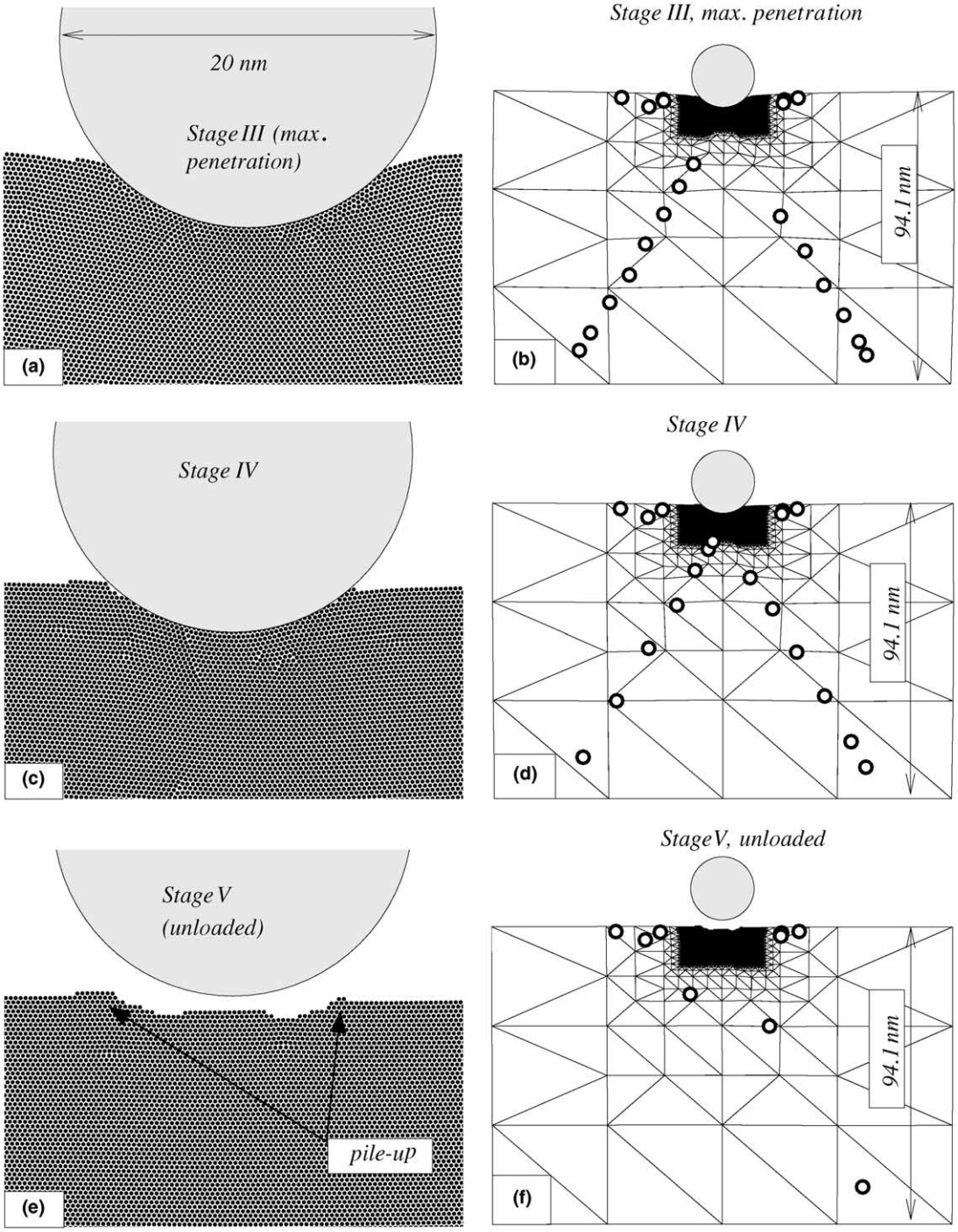

Fig. 8. Configuration of the atomic region ((a), (c) and (e)) and positions of the discrete dislocations ((b), (d) and (f)) at maximum load ((a)–(b)), during unloading ((c)–(d)) and after full unloading ((e)–(f)) for the displacement-controlled indentation of the thick film.

the unloading curve also appears close to the slope of the loading curve along those regions of the loading curve showing upward slope, i.e., in load ranges where no new dislocations are nucleated.

Beyond point IV in the unloading cycle, there is a significant change in slope of the unloading curve, which is coincident with dislocations gliding out of the top surface of the indenter or annihilating with other dislocations in the atomistic region. The critical load level at which this occurs will likely depend on both the inherent lattice resistance of the crystal (the Peierls stress), and on the various forces on the leading dislocation from other dislocations and from the indented and free surfaces. In this crystal, it is expected that the Peierls

stress should be quite low, but it is not generally possible to separate out the various contributions to the critical load.

The change in slope at point IV shows that the reverse plasticity does play an important role beyond a certain point, leading to a "Bauschinger" effect that is absent from standard continuum plasticity models. The existence of dislocations on multiple slip planes upon loading, a feature retained in the continuum region due to the maintenance of finite deformation behavior in the atomistic region, also leads to more-complex behavior on unloading; simple reverse motion and annihilation of pairs of dislocations does not occur. The reverse plasticity that we observe seems qualitatively similar to recent experimental observations of reverse plasticity in silicon nanospheres [11], where a significant fraction of the plastic deformation of the spheres during loading is recovered on unloading.

In addition, it is interesting to note that during the IV–V portion of the curve, dislocation *nucleation* is observed during *unloading*. Dislocations of opposite sign to those that formed during the loading stage nucleated during unloading and then quickly combined with pre-existing dislocations from the loading stage. This is contrary to the expectation that the unloading cycle would only involve the motion and annihilation of existing defects. This feature serves to further justify the need for full atomistic detail in localized regions of high deformation.

In the fully unloaded sample, at point V, there is clearly permanent deformation and flow of material, and atomic scale analogues of several larger-scale indentation features are evident. Most notably, Fig. 8(e) shows a pile-up of material on either side of the indenter that stands higher than the original undamaged surface. Analysis of the sequence of events forming this pile-up during the deformation reveals that the dislocation dissociation mechanism described earlier is key to the pile-up process. This suggests that in a 3D nanoindentation, pile-up requires a significant degree of cross-slip to take place during the deformation.

Upon complete unloading, several dislocations remain in the film. These are mainly the dislocations that dissociated and moved onto horizontal slip planes. Little, if any, of the signatures of plastic deformation remain when the atoms are viewed (Fig. 8(e)), and yet the pile-up belies the existence of material flow. In fact, the final deformation state, relative to the initial crystal, is highly deformed. Fig. 9 shows the deformed "elements" in the atomistic region after complete unloading, which makes clear that the nearly perfect atomic arrangement seen in Fig. 8(e) is associated with extensive reverse motion of dislocations on multiple slip planes, leading to the pile-ups. These simulations also suggest that careful interpretation of post-indentation simulations and experiments is required, since the extent of the plastic zone

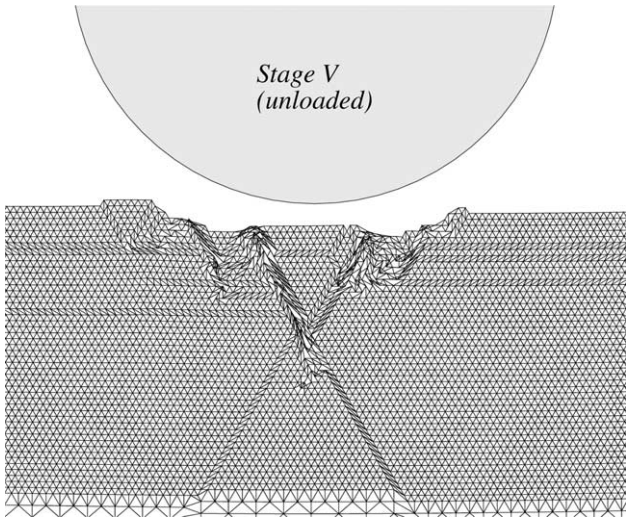

Fig. 9. Region under the indenter after unloading, showing the deformed elements rather than the atoms (cf. Fig. 8 (e)) to highlight the extensive plasticity which takes place.

which existed at maximum penetration depth is clearly substantially larger than that which remains after final unloading.

3.2. Force-controlled indentation of the "thick" film

For comparison, force-controlled boundary conditions were applied to the same simulation cell as that described in the previous section, so as to make better contact with a common experimental mode used in AFM nanoindentation studies (e.g. [4,26]). Fig. 10 shows the P–δ curve for this simulation. Although this

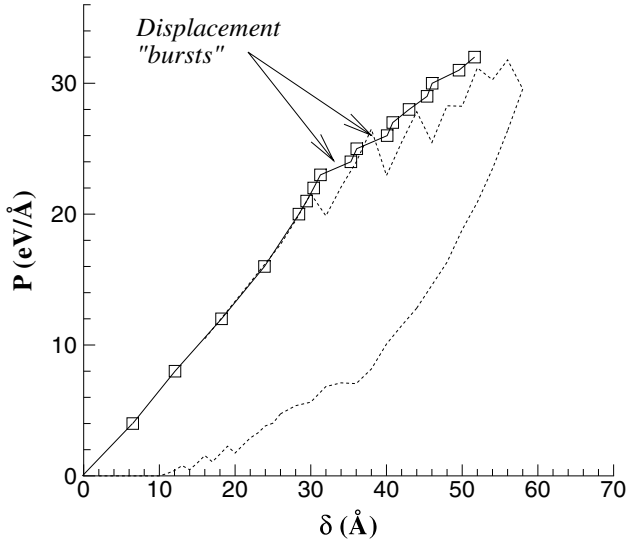

Fig. 10. Load–displacement curve for force-controlled indentation of the thick film, showing several displacement bursts corresponding to the nucleation and motion of dislocations. The dashed line is the displacement-controlled load–displacement curve from Fig. 4.

simulation was not loaded as highly as the displacement-controlled simulation nor was unloading investigated, two useful insights can be gained from these results. The first insight is that the nucleation and motion of dislocations occurs in essentially the same manner, starting at approximately the same load level and nucleation site, as in the displacement-controlled simulation. By the end of the force-controlled simulation, 12 dislocations have left the atomistic region (compared to 15 at about the same penetration depth in the displacement-controlled indentation).

The second insight is the clear existence of displacement "bursts" analogous to those seen in nanoindentation experiments. There has been some speculation in the nanoindentation literature that these bursts may be artifacts associated with the fracture of a brittle oxide layer on the material being indented, and corresponding doubts as to whether such bursts are evidence of homogeneous dislocation nucleation beneath the indenter. Our simulation has no oxide layer on the surface and thus provides additional evidence for the case that experimentally observed displacement bursts can indeed be caused by homogeneous nucleation of dislocations in the material. Fig. 11 shows the deformed atomistic region before and after the first displacement burst in the P–δ curve for the force-controlled indentation simulation, demonstrating the nucleation of two pairs of dislocations in that particular load step.

3.3. Displacement-controlled indentation of the "thin" film

Indentation into a much thinner film, such that the contact width of the indentation approaches the thickness of the film, exhibits slightly different behaviour than the indentation of the relatively thick film just described. In Fig. 12, the P–δ curve for the displacement-controlled indentation of the thin film is presented.

Up to point I on the P–δ curve, the response is completely elastic. Unlike for the thick film, comparison to Hertzian theory at I for the thin film shows significant effect of the substrate; this is not a surprising result given the small film thickness compared to the contact area and indenter radius. The first dislocation nucleates in the step from I to II, followed by several nucleation events until the maximum penetration at III is reached. The location of these nucleation events is approximately the same as in the simulation of the thick film, i.e., about

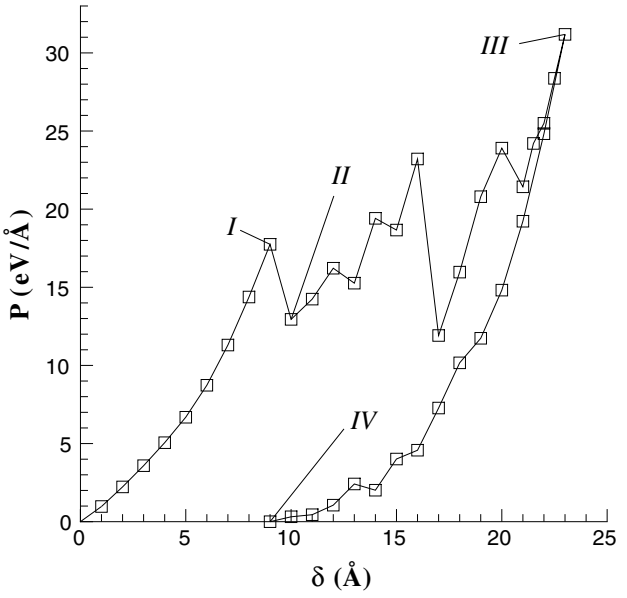

Fig. 12. Load–displacement curve for displacement-controlled indentation of the thin film. Points I–V are critical features described in the text.

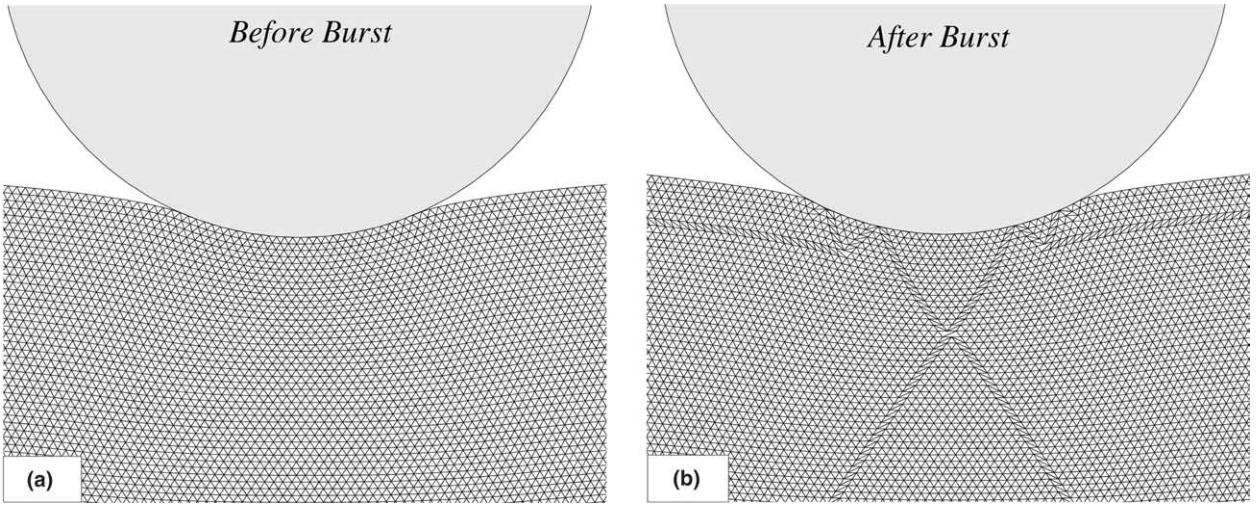

Fig. 11. Configuration of the atomistic region (a) before and (b) after the first "displacement burst" during the force-controlled indentation of the thick film. The mesh joining the atoms is shown, rather than the atoms themselves, to clearly show the burst of slip activity which occurs.

0.86a below the surface and on the centerline of the indenter.

Snapshots of the configuration at points III and IV are shown in Fig. 13. By point III, the dislocations have travelled long lateral distances after dissociating onto the horizontal glide planes, ranging from 120 to 350 Å left and right from the indenter. These long distances can be attributed to three effects: The low Peierls resistance for the discrete dislocations, the long-ranged nature of the stress fields due to 2D point-loading of a half-space, and the inability of the discrete dislocations to dissociate freely as they can when they are atomistic defects. On this last point, it is possible that the dislocations may want to dissociate due to the attraction of the free top surface and repulsion of the rigid substrate. While it is possible to include such dislocation reactions in the discrete dislocation formulation, the current implementation of CADD is not so equipped. Such dissociation would lead to dislocations leaving the surface of the crystal, giving rise to surface steps of the type recently observed using STM observations [7].

As for the thick film in Fig. 7 of Section 3.1, we plot the apparent hardness versus indentation depth for the thin film in Fig. 14. Unlike with the thick film, there is no clear evidence of a size effect for the thin film. In this case, there is no doubt a strong influence on the hardness from the close proximity of the rigid substrate.

It is interesting to examine the complex contact forces under the indenter throughout the indentation process. Fig. 15 shows the forces at the maximum penetration of the indenter, superimposed on the deformed mesh. At this stage, the ratio of the contact half-width to the film thickness is substantial, $a/t = 0.8$. The forces represent the typical shape of the force distribution for a number of configurations examined after dislocations had emitted. These results suggest the existence of a small region in the center with an approximately Hertzian distribution of contact stresses, surrounded by a much more irregular distribution of forces. Note that this central region does not correspond to the area where no dislocations have reached the indented surface, as can be observed from the mesh shown between the atoms in Fig. 15.

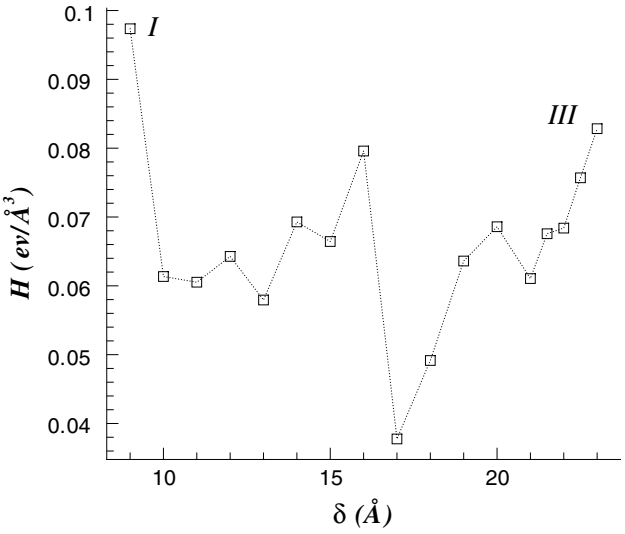

Fig. 14. Variation of hardness (load divided by contact area) with increasing indentation depth for the thin film.

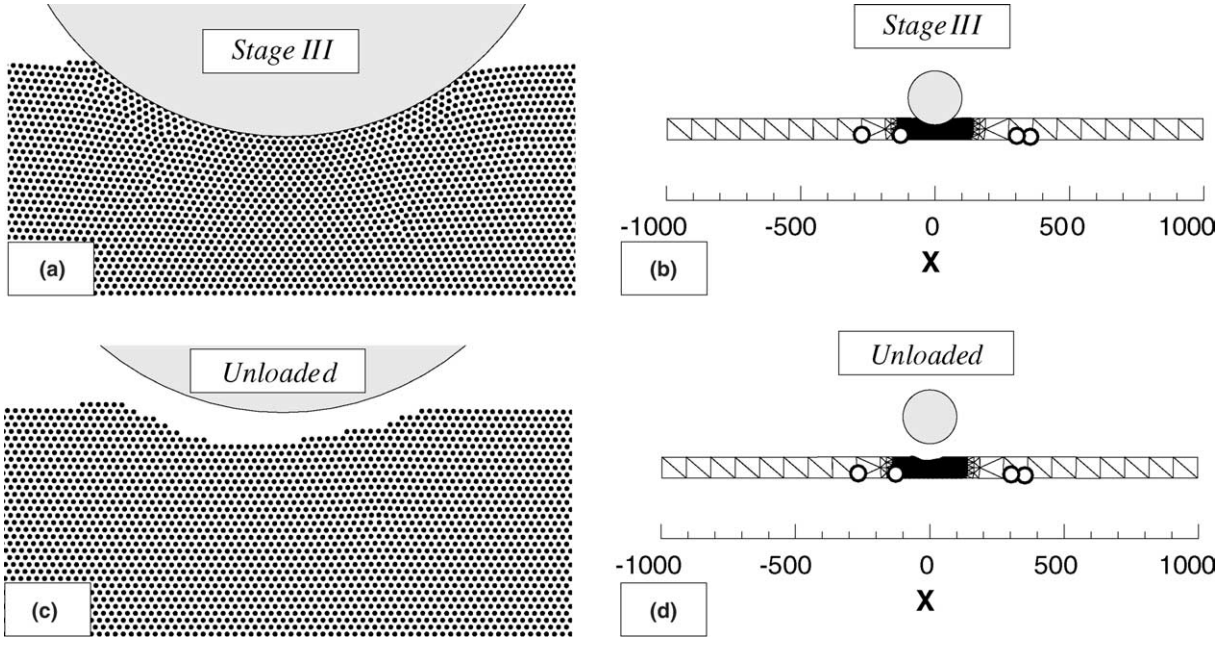

Fig. 13. Configuration of the atomic region ((a), (c)) and positions of the discrete dislocations ((b), (d)) at maximum load ((a)–(b)), and after unloading ((c)–(d)) for the displacement-controlled indentation of the thin film.

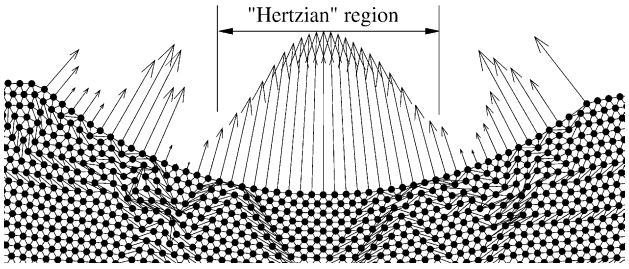

Fig. 15. Contact forces beneath the indenter at the point of maximum penetration (*III*) for the displacement-controlled thin film indentation.

The unloaded, damaged thin film is shown in Figs. 13(c) and (d). Note that the discrete dislocations remain in the film at approximately the same distance from the indenter as at maximum indenter penetration (point III). Also, comparing Fig. 13(c) with Fig. 8(e) shows that the final indentation takes on rather different shapes in the two cases. For the thin film, the indentation remains largely semi-circular, whereas there is a distinct trough on either side of the centerline in the thick film indentation. The mechanism responsible for this difference is the availability of appropriate dislocations during the unloading cycle. For the thick film, the pile-up of dislocations against the lower substrate reverse direction and ultimately eject through the surface of the material directly beneath the indenter, and carry with them material which creates the "bump" in the center of the indentation. For the thin film, many of the dislocations created during the loading cycle have moved onto the horizontal slip planes, and therefore are not easily attracted back to the surface during unloading.

4. Conclusions

In this paper, we have made use of the recently developed CADD method to study 2D nanoindentation by a frictionless cylindrical indenter into an initially defect-free single crystal films. In addition to the usual advantage of coupled methods, i.e., the reduction of the computational overhead compared to atomistic simulation, CADD permits the existence of continuum dislocations and plastic flow in the continuum region, allows for the transfer of dislocations back and forth across the atomistic/continuum interface in a seamless manner, and provides enhanced ability to track the details of defect nucleation and evolution as the simulation proceeds. These abilities have allowed us to make a number of more-quantitative observations about the deformation process than has been the case with fully atomistic simulations.

Briefly, we recount the wide range of results and observations found here:

1. As has been observed by others in direct atomistic simulations [13,18,29], homogeneous dislocation nucleation occurs below the surface, but not at the location of the maximum resolved shear stress on the crystal slip systems.
2. For the "thick" film (a 941 Å film and a 100 Å indenter radius), the material hardness is found to scale with indentation depth in a manner consistent with experimental studies at larger scales, suggesting that the size effect is not due to microstructural features but rather to the intrinsic evolution of the defect structure under the indentation loading. At the same time, indentation into a very thin film (a 78.5 Å film and a 100 Å indenter radius) shows no clear size effect.
3. Dislocation dissociation, the 2D analogue of cross-slip in 3D, is observed underneath the indenter and plays a key role in determining the subsequent overall deformation.
4. Initial unloading is essentially elastic in spite of reverse motion of previously emitted dislocations. Near complete unloading, a substantial Bauschinger effect, or change in the unloading curve slope, is observed and corresponds to the point at which dislocations begin to move out of the crystal or annihilate.
5. Dislocation nucleation was observed during unloading.
6. Upon complete unloading, only a small number of dislocations remain in the film, mainly those that had undergone dissociation and had moved laterally and near to the surface of the indented crystal.
7. In force-controlled indentation experiments, events of dislocation nucleation can clearly be correlated to displacement "bursts" observed in the P–δ curves.
8. The dislocation structures differ between thick and thin films, with dislocations in the thin film forced to move long lateral distances on horizontal slip planes, leading to distinct differences in the shape of the final indentation after unloading.

There are a range of extensions of the present study to address other issues associated with nanoindentation of single crystals. For instance, dislocation sources can be introduced into the continuum, to permit plasticity from pre-existing sources rather than from homogeneous nucleation alone. The effect of crystal orientation is easily investigated. The consequences of a Peierls barrier or phenomenological dislocation pinning interactions to impede the motion of the continuum dislocations can be investigated. The effect of indenter-substrate interactions on all of the phenomena listed above can be studied. Larger system sizes are also easily accessible. Finally, further load/unload cycles can be performed to investigate the evolution of cyclic deformation and material response.

At the outset of this paper, nanoindentation of nanocrystals was raised as a key area for both modeling and experiments. The influence of nanostructural defects, such as grain boundaries and surface steps, is of

considerable importance in determining the nanoindentation response and dislocation plasticity. While this has recently been investigated to some degree by other researchers (e.g. [17,21,32,33]) using fully atomistic models, the CADD model can be applied to such problems as well and likely will permit additional insights to be gained on the physical nature of nanocrystalling response. To do so requires extending CADD to treat multiple grains and the accompanying grain boundaries, which we have already accomplished in principle in unpublished work.

Many extensions to the basic CADD concept are feasible. We are currently extending CADD to a molecular-dynamics/dislocation-dynamics framework. This will permit a wide range of finite temperature, thermal activation, and dynamic or rate-dependent phenomena to be investigated. Such a dynamic CADD model can in principle be combined with accelerated MD methods to bridge scales in both time and space simultaneously. A final important direction for future work is to extend CADD to a 3D formulation. The atomistic/continuum coupling with dislocation loops wholly contained in one region or the other is not a major conceptual problem. However, the description of single dislocation loops as partly atomistic and partly continuum in nature, and the related passing of dislocation segments across the atomistic/continuum boundary is a major challenge. A 3D CADD model will also require implementation of a parallel computing framework. In spite of the difficulty, the payoff of a truly 3D multiscale method such as CADD opens the doors to extensive simulations of complex deformation processes in plastically deforming materials.

Acknowledgements

The authors gratefully acknowledge support of this work by the US Air Force Office of Scientific Research, Grant #F49620-99-1-0272, under the MURI program entitled "Virtual Design and Testing of Materials: a Multiscale Approach" at Brown University. R.M. also thanks the NSERC of Canada for financial support.

References

[1] Abraham FF, Broughton JQ, Bernstein N, Kaxiras E. Spanning the length scales in dynamic simulation. Comput Phys 1998;12:538.

[2] Born M, Huang K. Dynamical theory of crystal lattices. Oxford: Clarendon; 1954.

[3] Christopher D, Smith R, Richter A. Atomistic modelling of nanoindentation in iron and silver. Nanotechnology 2001;12:372–83.

[4] Corcoran SG, Colton RJ, Lilleodden ET, Gerberich WW. Anomalous plastic deformation at surfaces: nanoindentation of gold single crystals. Phys Rev B 1997;55(24):R16057–60.

[5] Curtin WA, Miller RE. Atomistic/continuum coupling in computational materials science. Modeling Simul Mater Sci Eng 2003;11(3):R33–R68.

[6] Daw MS, Baskes MI. Embedded-atom method: derivation and application to impurities, surfaces, and other defects in metals. Phys Rev B 1984;29:6443–53.

[7] de la Fuente OR, Zimmerman JA, Gonzalex MA, de la Figuera J, Hamilton JC, Pai WW, Rojo JM. Dislocation emission around nanoindentations on a (0 0 1) fcc metal surface studied by scanning tunneling microscopy and atomistic simulations. Phys Rev Lett 2002;88(3):036101.

[8] Ercolessi F, Adams JB. Interatomic potentials from first-principles calculations – the force-matching method. Europhys Lett 1994;26:583.

[9] Gerberich WW, Nelson JC, Lilleodden ET, Anderson P, Wyrobek JT. Indentation induced dislocation nucleation: the initial yield point. Acta Mater 1996;44(9):3585–98.

[10] Gerberich WW, Kramer DE, Tymiak NI, Volinsky AA, Bahr DF, Kriese MD. Nanoindentation-induced defect-interface interactions: phenomena, methods and limitations. Acta Mater 1999;47(15):4115–23.

[11] Gerberich WW, Mook WM, Perrey CR, Carter CB, Baskes MI, Mukerjee R, Gidwani A, Heberlein J, McMurry PH, Girshick SL. Superhard silicon nanospheres. J Mech Phys Sol 2003;51:979–92.

[12] Gerberich WW, Tymiak NI, Grunlan JC, Horstemeyer MF, Baskes MI. Interpretations of indentation size effects. J Appl Mech 2002;69:433–42.

[13] Kelchner CL, Plimpton SJ, Hamilton JC. Dislocation nucleation and defect structure during surface indentation. Phys Rev B 1998;58(17):11085–8.

[14] Kiely JD, Houston JE. Nanomechanical properties of au (1 1 1), (0 0 1) and (1 1 0) surfaces. Phys Rev B 1998;57(19):12588–94.

[15] Kohlhoff S, Gumbsch P, Fischmeister HF. Crack propagation in bcc crystals studied with a combined finite-element and atomistic model. Philos Mag A 1991;64(4):851–78.

[16] Lilleodden ET, Zimmerman JA, Foiles SM, Nix WD. An experimental and computational study of the elastic–plastic transition in thin films. Mater Res Soc Symp Proc 2001;673:P1.3.1–6.

[17] Lilleodden ET, Zimmerman JA, Foiles SM, Nix WD. Atomistic simulations of elastic deformation and dislocation nucleation during nanoindentation. J Mech Phys Sol 2003;51:910–20.

[18] Miller RE, Acharya A. A stress-gradient based criterion for dislocation nucleation in crystals. Philos Mag A [submitted to the Journal of the Mechanics and Physics of Solids].

[19] Miller RE, Shilkrot L, Curtin WA. A study of nano-indentation using coupled atomistic and discrete dislocation (cadd) modeling. In: Proceedings of the Second MIT Conference on Computational Fluid and Solid Mechanics; 2003 [in press].

[20] Rudd RE, Broughton JQ. Concurrent coupling of length scales in solid state systems. Phys Stat Sol B 2000;217:251–91.

[21] Shenderova O, Mewkill J, Linehan P, Brenner DW, Jarausch K, Russell PE. An evaluation of atomic force microscopy as a probe of nanoscale residual stress via atomistic simulation. Mater Res Soc Symp Proc 1998;522:233–8.

[22] Shenoy VB, Miller R, Tadmor EB, Phillips R, Ortiz M. Quasicontinuum models of interfacial structure and deformation. Phys Rev Lett 1998;80(4):742–5.

[23] Shenoy VB, Miller R, Tadmor EB, Rodney D, Phillips R, Ortiz M. An adaptive methodology for atomic scale mechanics: The quasicontinuum method. J Mech Phys Sol 1998;47:611–42.

[24] L.E. Shilkrot, R.E. Miller, W.A. Curtin, Coupled atomistic and discrete dislocation plasticity, Phys. Rev. Lett. 89 (2) (2002) 025501-1–025501-4.

[25] Shilkrot LE, Miller RE, Curtin WA. Multi-scale plasticity modeling: coupled atomistics and discrete dislocation mechanics. J Mech Phys Solids [in press].

[26] Suresh S, Nieh T-G, Choi BW. Nano-indentation of copper thin films on silicon substrates. Scripta Mater 1999;41(9):951–7.
[27] van der Giessen E, Needleman A. Discrete dislocation plasticity: a simple planar model. Modeling Simul Mater Sci Eng 1995;3:689–735.
[28] Vashishta P, Bachlechner M, Nakano A, Campbell TJ, Kalia RK, Kodiyalam S, Ogata S, Shimojo F, Walsh P. Multimillion atom simulation of materials of parallel computers – nanopicel, interfacial fracture, nanoindentation and oxidation. Appl Surf Sci 2001;182:258–64.
[29] VanVliet KJ, Li J, Zhu T, Yip S, Suresh S. Quantifying the early stages of plasticity through nanoscale experiments and simulations. Phys Rev B 2003;67:104105.
[30] Yang W, Tan H, Guo T. Evolution of crack tip processes. Modeling Simul Mater Sci Eng 1994;2:767–82.
[31] Zielinski W, Huang H, Gerberich WW. Microscopy and microindentation mechanics of single crystal fe-3 wt% si: Part ii. tem of the indentation plastic zone. J Mater Res 1993;8(6): 1300–10.
[32] Zimmerman JA, Kelchner CL, Klein PA, Hamilton JC, Foiles SM. Surface step effects on nanoindentation. Phys Rev Lett 2001;87(16):165507.
[33] Zimmerman JA, Klein PA, Foiles SM. Effect of surface steps on dislocation structure during nanoindentation. Mater Res Soc Symp Proc 2001;649:Q8.8.1–6.